Journal of Solid State Chemistry 185 (2012) 107–116

Contents lists available at SciVerse ScienceDirect

Journal of Solid State Chemistry

journal homepage: www.elsevier.com/locate/jssc

Structures of ordered tungsten- or molybdenum-containing quaternary perovskite oxides

Bradley E. Day [a], Nicholas D. Bley [a], Heather R. Jones [a], Ryan M. McCullough [a], Hank W. Eng [b,c], Spencer H. Porter [d], Patrick M. Woodward [d], Paris W. Barnes [a,*]

[a] Department of Chemistry, Millikin University, 1184 W. Main Street, Decatur, IL 62522, United States
[b] Department of Natural Sciences, San Antonio College, 1300 San Pedro Avenue, San Antonio, TX 78212, United States
[c] Department of Natural Sciences, St. Philip's College, 1801 Martin Luther King Drive, San Antonio, TX 78203, United States
[d] Department of Chemistry, The Ohio State University, 100 W. 18th Avenue, Columbus, OH 43210, United States

ARTICLE INFO

Article history:
Received 18 September 2011
Received in revised form
1 November 2011
Accepted 3 November 2011
Available online 12 November 2011

Keywords:
Quaternary perovskite
Double perovskite
Crystal structure and symmetry
X-ray powder diffraction
Neutron powder diffraction

ABSTRACT

The room temperature crystal structures of six A_2MMoO_6 and A_2MWO_6 ordered double perovskites were determined from X-ray and neutron powder diffraction data. Ba_2MgWO_6 and Ba_2CaMoO_6 both adopt cubic symmetry (space group $Fm\bar{3}m$, tilt system $a^0a^0a^0$). Ba_2CaWO_6 has nearly the same tolerance factor ($t=0.972$) as Ba_2CaMoO_6 ($t=0.974$), yet it surprisingly crystallizes with $I4/m$ symmetry indicative of out-of-phase rotations of the MO_6 octahedra about the c-axis ($a^0a^0c^-$). Sr_2ZnMoO_6 ($t=0.979$) also adopts $I4/m$ symmetry; whereas, Sr_2ZnWO_6 ($t=0.976$) crystallizes with monoclinic symmetry ($P2_1/n$) with out-of-phase octahedral tilting distortions about the a- and b-axes, and in-phase tilting about the c-axis ($a^-a^-c^+$). Ca_2CaWO_6 ($t=0.867$) also has $P2_1/n$ symmetry with large tilting distortions about all three crystallographic axes and distorted CaO_6 octahedra. Analysis of 93 double perovskites and their crystal structures showed that while the type and magnitude of the octahedral tilting distortions are controlled primarily by the tolerance factor, the identity of the A-cation acts as the secondary structure directing factor. When $A=Ba^{2+}$ the boundary between cubic and tetragonal symmetries falls near $t=0.97$, whereas when $A=Sr^{2+}$ this boundary falls somewhere between $t=1.018$ and $t=0.992$.

© 2011 Elsevier Inc. All rights reserved.

1. Introduction

In 2003, Eng et al. initiated a study of ternary and quaternary metal oxides containing metal cations with d^0 electron counts and their electronic structures [1]. Their rationale was to examine the optical properties of these compounds in an attempt to tune their band gaps chemically in search of a substance with better photocatalytic properties than TiO_2 [2]. Of the thirty-two compounds studied by Eng and co-workers, twenty-four compositions were reported to crystallize with the ordered double perovskite structure. The $A_2MM'X_6$ double perovskites are an extensively studied family of materials derived from the simple perovskite structure (AMX_3). The ideal cubic simple perovskite has $Pm\bar{3}m$ symmetry ($Z=1$; $a_p\sim4$ Å). As shown in Fig. 1, the simple perovskite is "doubled" by rock-salt ordering of equimolar amounts of two different M-cations on the octahedral coordination sites, the space group symmetry changes to $Fm\bar{3}m$ and the unit cell dimensions are doubled [3–5]. The most common distortion of the double perovskite structure occurs through cooperative tilting of the corner-sharing octahedra. If the A-cation that resides in the cavity formed by the $MM'O_6$ octahedral network is too small, the polyhedra can rotate cooperatively to accommodate the size mismatch while maintaining their corner-sharing connectivity [6,7]. Octahedral tilting distortions will be described throughout this paper using Glazer notation [8].

Here, we describe the crystal structures of six compounds containing W^{6+} or Mo^{6+} as determined from neutron and X-ray powder diffraction data. Correctly identifying the presence and details of octahedral tilting in ordered double perovskites is complicated by two factors. First, perovskites are prone to exhibit a high degree of pseudosymmetry, which can make it difficult to resolve peak splitting. Second, the superlattice reflections that arise from M/M' cation ordering overlap with the superlattice reflections that arise from out-of-phase octahedral tilting, which can mask the presence of octahedral tilting. Bearing these challenges in mind, powder diffraction data were analyzed in the same manner as used to study a number of double perovskites containing either Nb^{5+}, Ta^{5+}, or Sb^{5+} [9–13]. Interestingly the results presented here show several examples where A_2MMoO_6 and A_2MWO_6 perovskites with the nearly the same tolerance factor exhibit different patterns of octahedral tilting at room temperature.

* Corresponding author. Fax: +1 217 362 6408.
E-mail address: pbarnes@millikin.edu (P.W. Barnes).

0022-4596/$ - see front matter © 2011 Elsevier Inc. All rights reserved.
doi:10.1016/j.jssc.2011.11.007

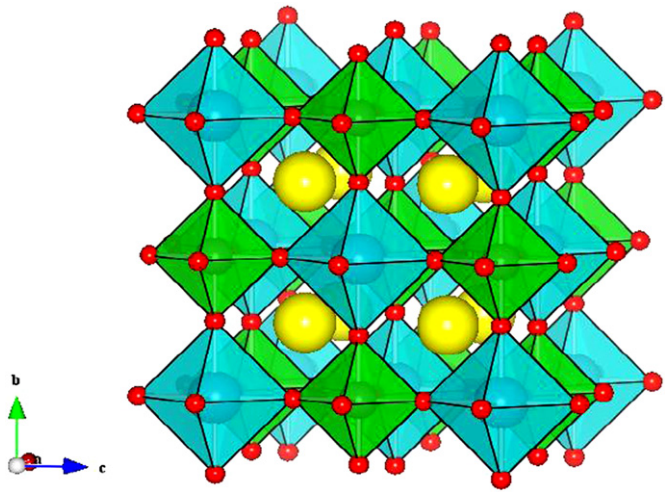

Fig. 1. Structure of Ba_2CaMoO_6 (space group: $Fm\bar{3}m$; tilt system: $a^0a^0a^0$). Legend: Ba: yellow spheres; O: red spheres; [CaO_6]: blue octahedra; [MoO_6]: green octahedra. All structural figures were created with the VESTA software, version 2.0 [40].

2. Experimental

2.1. Synthesis

Polycrystalline samples were prepared from high (>99.9%) purity $BaCO_3$, $SrCO_3$, $CaCO_3$, MgO, ZnO, CdO, MoO_3 and/or WO_3 by conventional solid-state techniques. Stoichiometric amounts of the appropriate alkaline earth metal carbonates and metal oxides were weighed and mixed in an agate mortar and pestle. Acetone was added to the powders to facilitate mixing. The loose powdered reaction mixtures were added to high form alumina crucibles and heated between 800 and 900 °C overnight to decompose the carbonates. After pre-heating the reaction mixture, the powders were ground and reheated multiple times until the samples were homogeneous. Final sintering temperatures for all samples were between 1000 and 1350 °C [1].

2.2. Powder diffraction data collection and analysis

After high purity samples were made, refineable X-ray powder diffraction (XRPD) data were collected using a Bruker Advance D8 equipped with a position sensitive detector (PSD). Data were collected from 10° to 120° 2θ with a step size of ~0.015° at a rate of 2 s step^{-1} using monochromatic Cu $K\alpha_1$ radiation (λ=1.54056 Å; 40 kV, 50 mA). Rietveld refinements of the XRPD data were completed using the Total Pattern Analysis Software (TOPAS) package [14].

High resolution time-of-flight neutron powder diffraction (NPD) data were collected at the Special Environmental Powder Diffractometer (SEPD) at Argonne National Laboratory [15]. Complete Rietveld refinements on data collected using detector banks #1 and #2 (2θ=144° and 90°, respectively) were completed using the EXPGUI/GSAS software package [16,17]. Starting models for all compositions were generated by the perovskite structure prediction software SPuDS [6,18].

3. Results

3.1. Ba_2MgWO_6 and Ba_2CaMoO_6

Steward and Rooksby [19] first reported the synthesis and lattice parameters of Ba_2MgWO_6 (t=1.038) and Ba_2CaMoO_6 (t=0.974). When indexing the reflections associated with each compound, they noted that the X-ray diffraction data for Ba_2CaMoO_6 showed no reflection splitting or broadening and therefore, did not deviate from cubic symmetry. However, they believed Ba_2MgWO_6 deviated slightly from cubic symmetry due to the presence of weak extra reflections. Additional structural reports conclude that both Ba_2MgWO_6 [19–26] and Ba_2CaMoO_6 [21,27] crystallize with the cubic, fully ordered double perovskite structure.

Reflection indexing confirmed that data sets collected on these compounds contained only sublattice (all even h, k, and l values) and superlattice R-point (all odd h, k, and l values) reflections indicative of space group symmetries associated with either no tilting ($a^0a^0a^0$) or out-of-phase tilting (*e.g.*, $a^0a^0c^-$, $a^0b^-b^-$, $a^-a^-a^-$). Although there was no indication of peak splitting, refinements for both compounds were carried out with $Fm\bar{3}m$ ($a^0a^0a^0$), $I4/m$ ($a^0a^0c^-$), $I2/m$ ($a^0b^-b^-$), and $R\bar{3}$ ($a^-a^-a^-$) models. The lack of reflection splitting and the comparable fits between the four structural models allowed us to conclude that both compounds adopt $Fm\bar{3}m$ symmetry. The refined crystal structures of Ba_2MgWO_6 and Ba_2CaMoO_6 are reported in Table 1 and the cubic structure is illustrated in Fig. 1. The Rietveld fit of the neutron diffraction pattern for Ba_2CaMoO_6 is shown in Fig. 2.

3.2. Sr_2ZnMoO_6 and Ba_2CaWO_6

Sr_2ZnMoO_6 (t=0.979) was previously described as a distorted perovskite but only pseudo-cubic lattice parameters were reported [19]. Later, the crystal structure of Sr_2ZnMoO_6 was reported as tetragonal, although it was reported at $P4mm$ [28]. $P4mm$ symmetry in perovskites results from cooperative out-of-center displacements of the cations along a 4-fold axis, as it does in the tetragonal structures of $BaTiO_3$ [29] and $PbTiO_3$ [30]. Such distortions are highly unlikely for Sr_2ZnMoO_6. Octahedral tilting is much more likely to be responsible for lowering the symmetry from the cubic $Fm\bar{3}m$ symmetry of the parent structure.

The earliest report of the synthesis and crystal structure of Ba_2CaWO_6 (t=0.972) was by Steward and Rooksby in 1951 [19]. They reported that much like Ba_2CaMoO_6, the tungsten analog was cubic even though the tolerance factors for both compounds

Table 1
Room temperature structures of Ba_2MgWO_6 and Ba_2CaMoO_6 was determined from neutron powder diffraction data. The space group symmetry is $Fm\bar{3}m$. Goodness of fit parameters are reported for data collected using the 144° and 90° detector banks. Atomic positions are Ba (8*c*—¼, ¼, ¼), *M* (4*a*—0, 0, 0), *M*′ (4*b*—½, 0, 0), and O (24*e*—*x*, 0, 0).

	Ba_2MgWO_6	Ba_2CaMoO_6
R_p	5.28 5.47	4.85 4.64
R_{wp}	8.21 8.48	7.49 7.48
$R(F^2)$	4.19 4.33	5.59 6.00
χ^2	1.791	1.729
Lattice parameters		
a (Å)	8.10838(6)	8.38011(3)
Atomic coordinates		
O (x)	0.26202(5)	0.27184(5)
Displacement parameters (Å^2; ×100)		
U_{iso} (Ba)	0.48(1)	0.89(2)
U_{iso} (M)	0.65(3)	0.48(3)
U_{iso} (M')	0.42(3)	0.46(2)
U_{11} (O)	0.42(2)	0.47(2)
U_{22} (=U_{33}; O)	0.91(2)	2.17(2)

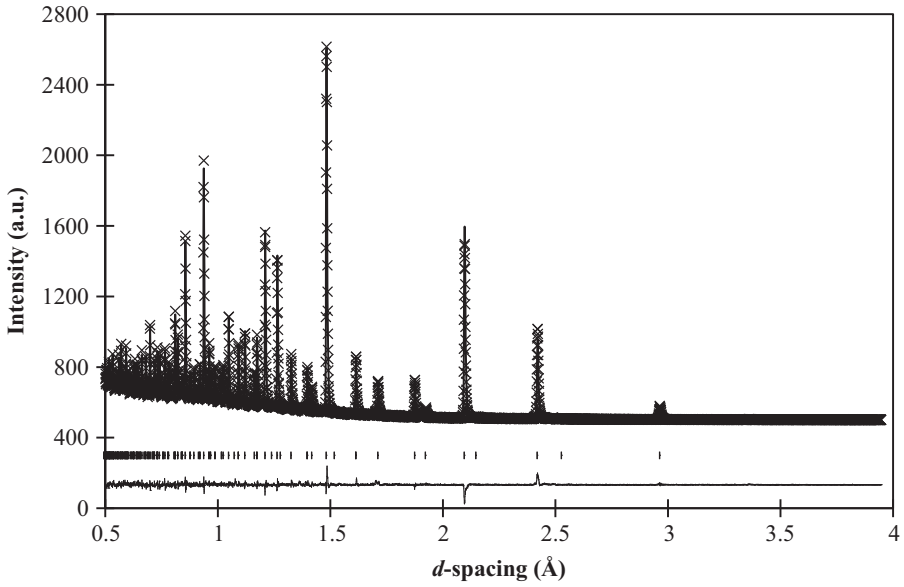

Fig. 2. Neutron diffraction pattern collected for Ba_2CaMoO_6. The data shown was collected using the 144° backscatter detector bank. Vertical bars shown below the fitted data indicate the *d*-spacing of the observed reflections.

Table 2
Room temperature structure of Sr_2ZnMoO_6 determined from neutron powder diffraction data. The space group symmetry is *I*4/*m*. The lattice parameters are $a=5.5867(3)$ Å and $c=7.9862(4)$ Å. Goodness of fit parameters are reported for data collected using the 144° and 90° detector banks are $R_p=4.27$ and 4.54%, $R_{wp}=6.57$ and 7.18%, $R(F^2)=4.91$ and 7.81%, and $\chi^2=2.476$.

Atom	Site	*X*	*y*	*z*	*U* (Å²; ×100)
Sr	4*d*	0	½	¼	0.88(2)
Zn	2*a*	0	0	0	0.71(2)
Mo	2*b*	½	½	0	0.17(2)
O(1)	4*e*	0	0	0.2613(2)	$U_{11}=U_{22}=1.92(4)$ $U_{33}=0.37(5)$
O(2)	8*h*	0.2260(2)	0.2939(1)	0	$U_{11}=0.60(4)$; $U_{22}=0.92(4)$ $U_{33}=1.91(4)$; $U_{12}=-0.35(3)$

were less than 1. Subsequent reports supported the claim that Ba_2CaWO_6 adopted $Fm\bar{3}m$ symmetry [20–22,27,31] until Yamamura and co-workers observed peak splitting at high angles. They stated that Ba_2CaWO_6 crystallized with *I*4/*m* symmetry. This space group assignment based upon the observation of sublattice reflection splitting at ~95° 2θ into the 008 and 440 reflections in laboratory XRPD data [32].

Analysis of the XRPD and NPD data for Sr_2ZnMoO_6 shows clear splitting of the sublattice peaks without additional *M*-point or *X*-point reflections. The *R*-point reflections arise from Zn/Mo ordering and out-of-phase tilting distortions. Additionally, since the tolerance factor is slightly below one, *I*4/*m* symmetry ($a^0a^0c^-$) is a reasonable assignment. The refined crystal structure of Sr_2ZnMoO_6 is given in Table 2. The *I*4/*m* structure is illustrated in Fig. 3 and the Rietveld fit to the Sr_2ZnMoO_6 neutron diffraction data is shown in Fig. 4.

Upon cursory glance, the XRPD and NPD diffraction data for Ba_2CaWO_6 suggest that this compound is cubic and isostructural with Ba_2CaMoO_6. However, close examination of high angle reflections in the X-ray diffraction data reveals subtle deviations from cubic symmetry. Splitting of the cubic 800 and 840 reflections is observed, as shown in Fig. 5. Complete Rietveld refinements were carried out on X-ray and neutron diffraction data

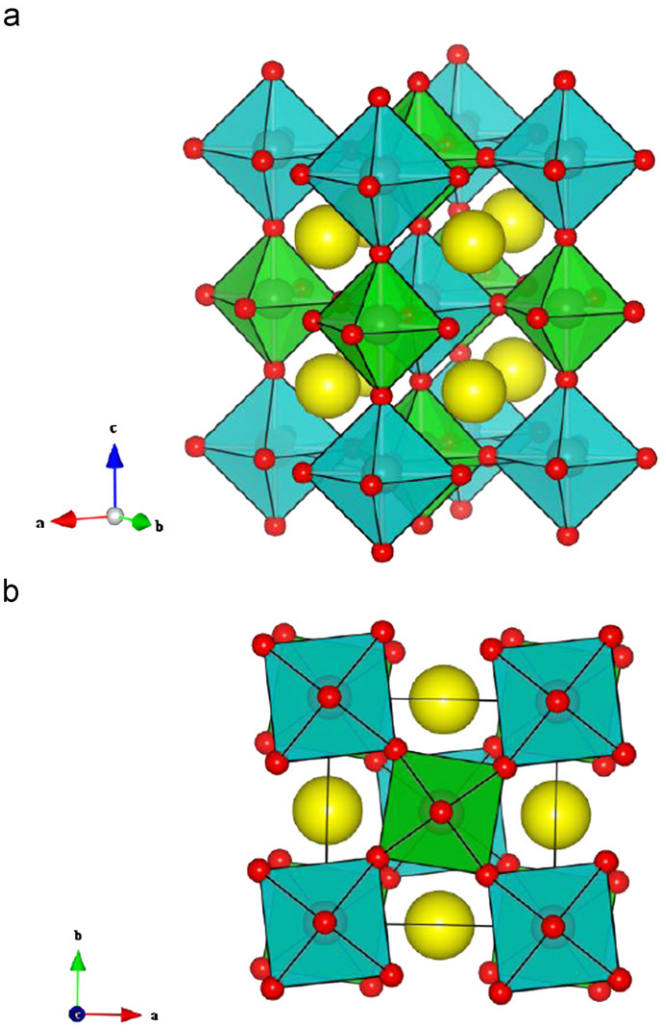

Fig. 3. (a) Structure of Sr_2ZnMoO_6 (space group: *I*4/*m*; tilt system: $a^0a^0c^-$). (b) Out-of-phase tilting occurs along the 001 direction. Legend: Sr: yellow spheres; O: red spheres; [ZnO_6]: blue octahedra; [MoO_6]: green octahedra.

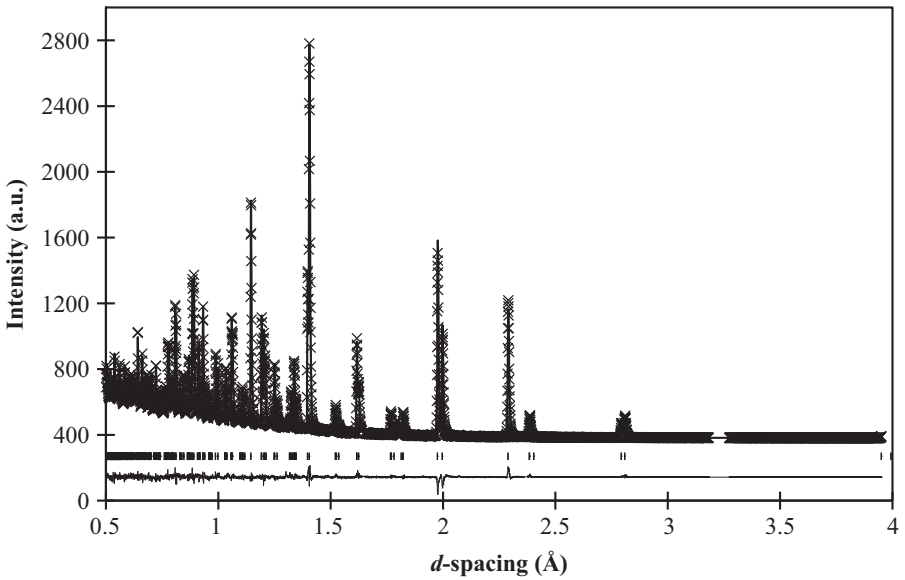

Fig. 4. Neutron diffraction pattern collected for Sr_2ZnMoO_6. The data shown was collected using the 144° backscatter detector bank. Vertical bars shown below the fitted data indicate the *d*-spacing of the observed reflections. A small impurity reflection observed at $d=3.23$ Å was excluded from the refined data.

using $a^0a^0a^0$ ($Fm\bar{3}m$), $a^0a^0c^-$ ($I4/m$), $a^0b^-b^-$ ($I2/m$), and $a^-a^-a^-$ ($R\bar{3}$) models. The goodness-of-fit parameters (χ^2) determined from refinement of the neutron diffraction data was 1.508 for the $I4/m$ model, 1.650 for the $I2/m$ model, and 1.491 for the $R\bar{3}$ model, and 1.569 for the $Fm\bar{3}m$ model. Theoretically, χ^2 should be equal for all four structural models, but this is not always observed. The high angle peak splitting observed in the XRPD was modeled most appropriately using the $I4/m$ model. The lack of reflection splitting observed below 94° 2θ in the XRPD is due to the pseudosymmetry of Ba_2CaWO_6. The $c/\sqrt{2}a$ ratio is equal to 1.001, similar to the lattice parameter ratios reported for pseudo-cubic perovskites Sr_2CrTaO_6 (0.9995) and Sr_2GaTaO_6 (0.9987), both of which also adopt $I4/m$ symmetry [9]. The refined crystal structure of Ba_2CaWO_6 is reported in Table 3.

3.3. Sr_2ZnWO_6 and Ca_2CaWO_6

Sr_2ZnWO_6 was originally reported to crystallize with tetragonal symmetry [28,33]. Later, the room temperature structure of Sr_2ZnWO_6 was reported using the monoclinic space group $C2/m$ [34]. More recently, the structure of Sr_2ZnWO_6 was reported as $P2_1/n$ by Gateshki et al. [35]. Ca_2CaWO_6 was first reported by Steward and Rooksby where they stated that its crystal structure was similar to Na_3AlF_6 [19,36]. The structure was later reported with the monoclinic $P2_1$ space group by Baglio and Natansohn [37]. Much like the erroneous space group assignment for Sr_2ZnMoO_6, $P2_1$ symmetry is probably incorrect because group theoretical analysis of the perovskite structure with cation ordering and cooperative tilting distortions of corner-sharing octahedra does not allow for this space group symmetry [7].

Reflection splitting patterns in the X-ray diffraction data of Sr_2ZnWO_6 and Ca_2CaWO_6 suggested both compounds can be indexed using an orthorhombic unit cell with dimensions $\sqrt{2}a_p \times \sqrt{2}a_p \times 2a_p$. Ordered perovskites can adopt orthorhombic symmetry (space group *Pnnn*), but the unit cell metrics must be $2a_p \times 2a_p \times 2a_p$. The metrics of the orthorhombic ordered perovskite cell are different than what we observed when indexing the diffraction data for both compounds. Additionally, all three types of sublattice reflections (*R*, *M*, and *X*) were observed in the neutron powder diffraction data (Fig. 6). This suggests that the correct space group assignment for both compounds is $P2_1/n$ ($a^-a^-c^+$; Fig. 7). The refined lattice parameters and atomic positions for these two compounds are given in Tables 4 and 5. The Rietveld fit to the Ca_2CaWO_6 NPD data is shown in Fig. 8.

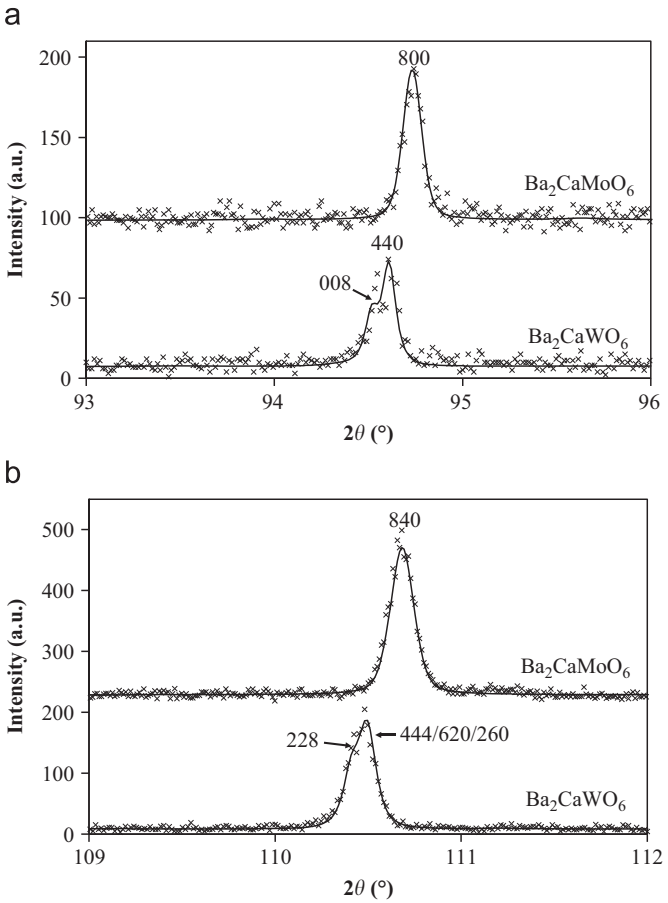

Fig. 5. Partial X-ray diffraction patterns for Ba_2CaMoO_6 and Ba_2CaWO_6. The solid lines represent the Rietveld fits to the collected data. The χ^2 values for the fits to the Ba_2CaMoO_6 and Ba_2CaWO_6 data were 1.12 and 1.17, respectively. Splitting is observed in *R*-type superlattice peaks of $BaCaWO_6$ at (a) ~94.5° and (b) ~110.5°. No peak splitting is observed in the diffraction data for Ba_2CaMoO_6 from 20° to 120° 2θ.

3.4. XRPD analysis of additional Mo^{6+} or W^{6+}-containing quaternary perovskites

Simultaneous use of neutron and X-ray powder diffraction when analyzing materials allows one to determine their structures with a high degree of confidence. Unfortunately, NPD is not always readily available or appropriate for certain elements, but as the previous results indicate careful inspection of the peak splitting and reflection conditions in the XRPD pattern when used in combination with the appropriate symmetry analysis can be reliably used to ascertain the tilt system of A_2MMoO_6 and A_2MWO_6 perovskites. Eleven additional molybdenum- or tungsten-containing perovskites were synthesized as previously reported in the chemical literature and analyzed using X-ray powder diffraction methods. The XRPD data was indexed using primitive cubic Miller indices according to the method outlined in Barnes et al. [9], and after an appropriate space group was determined, the data was analyzed using the Rietveld method. The space group symmetry and unit cell dimensions for these compositions are reported in Table 6. Atomic positions are not reported here because in perovskites that exhibit significant pseudosymmetry and possess heavy elements it is difficult to accurately locate the positions of the oxygen atoms using laboratory XRPD data.

Table 3
Room temperature structure of Ba_2CaWO_6 determined from neutron powder diffraction data. The space group symmetry is $I4/m$. The lattice parameters are $a=5.9374(3)$ Å and $c=8.4015(7)$ Å. Goodness of fit parameters are reported for data collected using the 144° and 90° detector banks are $R_p=4.79$ and 5.31%, $R_{wp}=7.72$ and 8.56%, $R(F^2)=5.43$ and 8.70%, and $\chi^2=1.508$.

Atom	Site	x	y	z	U (Å²; ×100)
Ba	4d	0	½	¼	0.81(2)
Ca	2a	0	0	0	0.56(3)
W	2b	½	½	0	0.40(3)
O(1)	4e	0	0	0.2733(6)	$U_{11}=U_{22}=1.9(2)$ $U_{33}=0.3(2)$
O(2)	8h	0.2619(4)	0.2793(5)	0	$U_{11}=1.6(2)$; $U_{22}=1.9(2)$ $U_{33}=1.6(2)$; $U_{12}=-1.2(1)$

4. Discussion

Selected bond lengths, bond angles, bond valence sums (BVS) [38], octahedron distortion indices, and polyhedral volumes are reported in Table 7 for all compounds whose structures were determined from NPD. The bond valence sums for Mo, W and O are consistently close (within 5%) to their ideal values, whereas larger deviations are observed for the A^{2+} and M^{2+} cations. For Ba_2MgWO_6, the response is what one might expect for a perovskite whose tolerance factor is 1.038. The Ba^{2+} cation resides in a twelve-coordinate hole that is too small. Therefore, the Ba–O bonds are too short and its BVS is too large (2.48). To accommodate this bond strain the Mg- and W-centered octahedra are stretched and the BVS for these cations (1.87 and 5.80, respectively) fall below their ideal values. This is effectively the only response available for a double perovskite whose tolerance factor is greater than unity.

The situation is less predictable for Ba_2CaMoO_6 ($t=0.974$) and Ba_2CaWO_6 ($t=0.972$). Here the tolerance factors less than unity, presenting two paths available to accommodate the bond strains that result from the mismatch in the sizes of the cations. One possibility is for the A–O bonds to stretch beyond their ideal lengths, making the A-site cation underbonded, while the M–O and/or M'–O cation bonds contract, making one or both of these cations overbonded. This is the path taken by Ba_2CaMoO_6 at room temperature, where we see that nearly all of the overbonding is

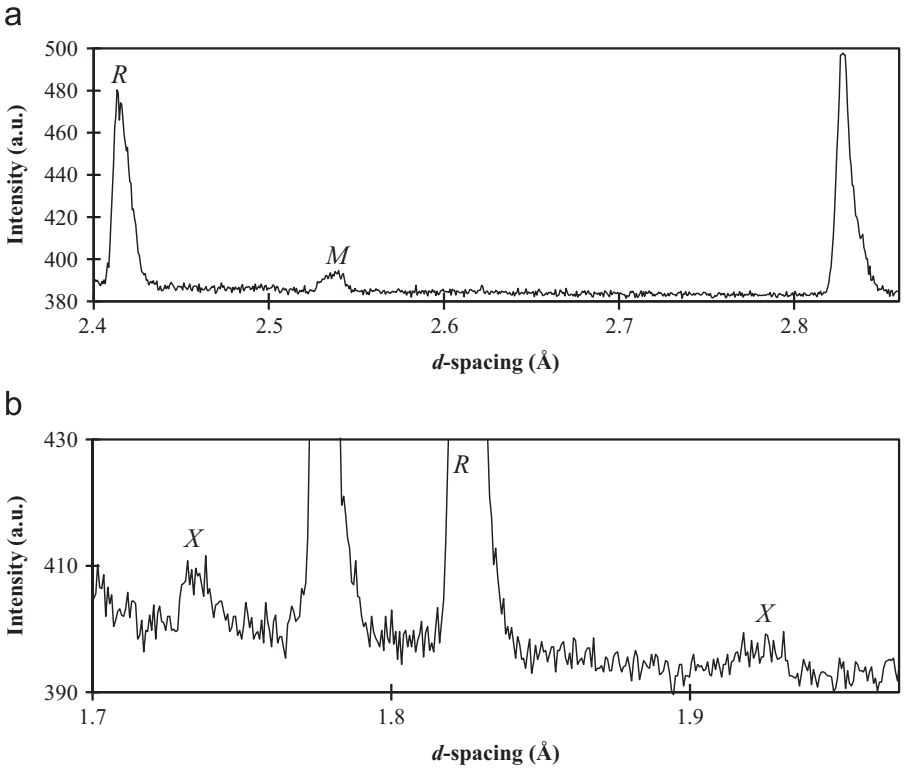

Fig. 6. Key superstructure reflections observed in the neutron diffraction data of Sr_2ZnWO_6 due to (a) in-phase octahedral tilting (marked M), out-of phase tilting and M-site cation ordering (R) and (b) coupled in-phase and out-of-phase tilting (X). Unmarked reflections are characteristic reflections associated with the basic perovskite sublattice.

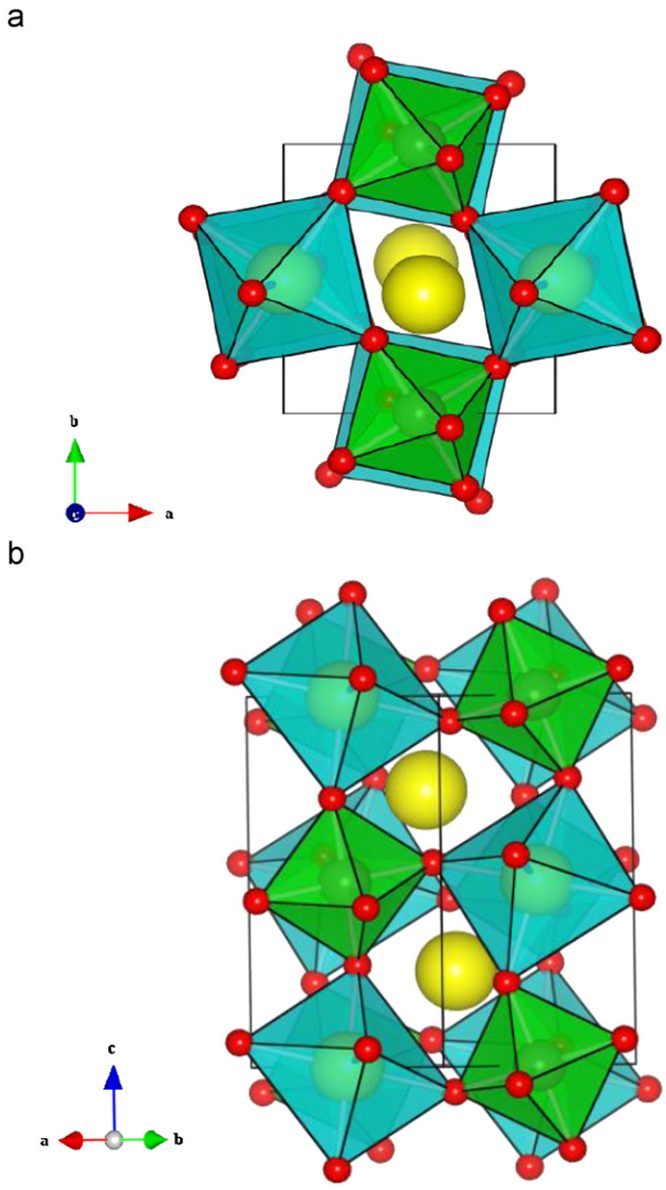

Fig. 7. (a) Structure of Ca_2CaWO_6 (space group: $P2_1/n$; tilt system: $a^-a^-c^+$) projected along the 010 direction, showing in-phase octahedral tilting and (b) the monoclinic structure projected along the 110 direction, showing out-of-phase octahedral tilting. Legend: Ca:yellow spheres; O:red spheres; [CaO_6]: blue octahedra; [WO_6]: green octahedra.

taken up by Ca^{2+} whose BVS is 2.59. The other possibility is to undergo an octahedral tilting distortion in order to raise the valence of the *A*-site cation. While Ba_2CaWO_6 does exhibit $a^0a^0c^-$ octahedral tilting, the distortion is so small that the valences of the ions are very similar to those found for cubic Ba_2CaMoO_6. Thus we can say that both compounds accommodate bond strains through expansion of the Ba–O bonds and compression of the Ca–O bonds. The similarity of the bond valences and large anisotropic thermal parameters for the lighter atoms supports the notion that both Ba_2CaMoO_6 and Ba_2CaWO_6 undergo a cubic ($Fm\bar{3}m$) to tetragonal ($I4/m$) transition near room temperature, but the transition temperatures are apparently slightly below room temperature for Ba_2CaMoO_6 and slightly above room temperature for Ba_2CaWO_6.

The variations in the BVS of the Ba^{2+} cations seen in Table 7 suggest that Ba–O bonds are reasonably flexible and can contract or expand, within certain limits, to maintain the symmetry of the cubic structure. It is also interesting to note that the overbonding of octahedrally-coordinated Ca^{2+} is found even in Ca_2CaWO_6 where the tolerance factor (t=0.867) is far below unity. At first glance this would seem to suggest some error in the bond valence parameters for the Ca–O bonds, yet the underbonding of the *A*-site Ca^{2+} ions in Ca_2CaWO_6 immediately bring this notion into question. This observation merits further investigation across a larger family of perovskites containing Ca^{2+}.

The regularity of octahedra can be measured using the distortion index (Δ_d). The distortion index compares the individual *M*–O bond lengths (d_n) to the average *M*–O length ($\langle d \rangle$):

$$\Delta_d = \frac{1}{6}\sum_{n=1,6}\left[\frac{d_n - \langle d \rangle}{\langle d \rangle}\right]^2$$

Octahedra with significant irregularities have Δ_d values greater than 10^{-3} [39]. For the compositions examined here, none of the ions should undergo electronic symmetry lowering distortions. Tilting distortions typically occur between nearly regular, rigid octahedra. Values of Δ_d would be zero if the octahedra were truly undistorted, but for lower symmetry space groups, small non-zero values are expected. Table 7 shows the distortion indices for octahedra in Ba_2CaWO_6, Sr_2ZnWO_6, and Sr_2ZnMoO_6 are relatively small, suggesting that their octahedra are minimally distorted. The small octahedral distortion indices, coupled with the fact that the O–*M*–O bond angles are approximately 90° in all compositions, reinforce the description that the distortions to lower symmetry are driven by rotations of rigid octahedra. The largest value of Δ_d is seen for the CaO_6 octahedra in Ca_2CaWO_6. The extent of distortion of the CaO_6 octahedra can also be seen in the O–Ca–O bond angles: O(1)–Ca–O(3)=94.83(3)° and O(2)–Ca–O(3)=95.08(3)°. The larger

Table 4
Room temperature structure of Sr_2ZnWO_6 determined from neutron powder diffraction data. The space group symmetry is $P2_1/n$. The lattice parameters are a=5.6321(3) Å, b=5.6080(3) Å, c=7.9265(4) Å, and β=89.962(1)°. Goodness of fit parameters are reported for data collected using the 144° and 90° detector banks are R_p=4.09 and 4.56%, R_{wp}=6.65 and 7.54%, $R(F^2)$=7.40 and 8.77%, and χ^2=1.713.

Atom	Site	*x*	*y*	*z*	*U* (Å²; ×100)
Sr	4*e*	0.5000(3)	0.5095(4)	0.2493(7)	0.87(2)
Zn	2*c*	0	½	0	0.59(4)
W	2*d*	½	0	0	0.31(4)
O(1)	4*e*	0.2741(7)	0.2530(6)	0.0234(7)	U_{11}=0.8(1); U_{22}=0.4(1) U_{33}=1.2(2); U_{12}=0.4(1) U_{13}=0.4(1); U_{23}=−0.1(1)
O(2)	4*e*	0.2420(8)	0.7796(6)	0.0259(7)	U_{11}=1.7(2); U_{22}=0.3(1) U_{33}=1.6(2); U_{12}=−0.5(1) U_{13}=0.2(2); U_{23}=0.0(1)
O(3)	4*e*	0.5491(3)	−0.0016(6)	0.2397(6)	U_{11}=0.90(8); U_{22}=1.7(1) U_{33}=0.5(1); U_{12}=−0.2(1) U_{13}=−0.1(1); U_{23}=−0.4(2)

Table 5
Room temperature structure of Ca_2CaWO_6 determined from neutron powder diffraction data. The space group symmetry is $P2_1/n$. The lattice parameters are $a=5.5518(3)$ Å, $b=5.8100(3)$ Å, $c=8.0066(4)$ Å, and $\beta=89.808(1)^\circ$. Goodness of fit parameters are reported for data collected using the 144° and 90° detector banks are $R_p=2.53$ and 2.50%, $R_{wp}=3.89$ and 3.85%, $R(F^2)=3.37$ and 4.24%, and $\chi^2=1.575$.

Atom	Site	x	y	z	U (Å²; ×100)
Ca(1)	4e	0.4852(2)	0.5569(1)	0.2558(2)	0.80(2)
Ca(2)	2c	0	½	0	0.56(3)
W	2d	½	0	0	0.48(3)
O(1)	4e	0.3335(1)	0.2751(1)	0.0694(1)	$U_{11}=0.89(4)$; $U_{22}=0.57(4)$ $U_{33}=1.11(5)$; $U_{12}=0.29(3)$ $U_{23}=0.07(3)$; $U_{13}=-0.32(4)$
O(2)	4e	0.2170(1)	0.8245(1)	0.0495(1)	$U_{11}=0.73(4)$; $U_{22}=0.82(4)$ $U_{33}=0.99(5)$; $U_{12}=-0.45(3)$ $U_{23}=0.29(4)$; $U_{13}=-0.32(3)$
O(3)	4e	0.6124(1)	−0.0526(1)	0.2254(1)	$U_{11}=0.88(4)$; $U_{22}=0.86(4)$ $U_{33}=0.46(4)$; $U_{12}=-0.11(3)$ $U_{23}=-0.02(3)$; $U_{13}=-0.01(4)$

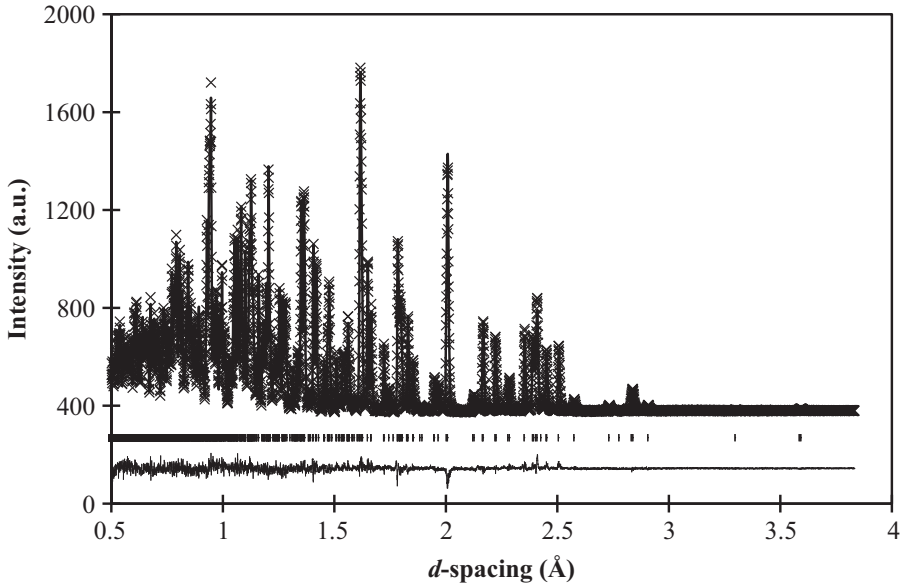

Fig. 8. Neutron diffraction pattern collected for Ca_2CaWO_6. The data shown was collected using the 144° backscatter detector bank. Vertical bars shown below the fitted data indicate the *d*-spacing of the observed reflections.

Table 6
Space groups, tolerance factors, and lattice parameters for perovskite compositions containing either Mo^{6+} or W^{6+} as obtained from analysis of laboratory X-ray powder diffraction data.

Compound	t	Space group	a (Å)	b (Å)	c (Å)	β (°)
Ba_2MgMoO_6	1.041	$Fm\bar{3}m$	8.08377(5)	–	–	–
Ba_2MgWO_6	1.038	$Fm\bar{3}m$	8.09849(5)	–	–	–
Ba_2ZnMoO_6	1.038	$Fm\bar{3}m$	8.10339(5)	–	–	–
Ba_2ZnWO_6	1.035	$Fm\bar{3}m$	8.11612(4)	–	–	–
Ba_2CdMoO_6	0.989	$Fm\bar{3}m$	8.32695(5)	–	–	–
Ba_2CdWO_6	0.986	$Fm\bar{3}m$	8.34120(6)	–	–	–
Sr_2MgMoO_6	0.982	$I4/m$	5.57039(2)	–	7.92447(3)	–
Sr_2MgWO_6	0.979	$I4/m$	5.58146(3)	–	7.93907(5)	–
Sr_2ZnMoO_6	0.979	$I4/m$	5.58282(3)	–	7.97927(5)	–
Sr_2ZnWO_6	0.976	$P2_1/n$	5.60704(7)	5.63171(5)	7.92487(8)	89.999(9)
Ba_2CaMoO_6	0.974	$Fm\bar{3}m$	8.37569(3)	–	–	–
Ba_2CaWO_6	0.972	$I4/m$	5.92946(4)	–	8.39171(1)	–
Sr_2CdWO_6	0.930	$P2_1/n$	5.7504(1)	5.8173(1)	8.1519(2)	89.952(7)
Ca_2MgWO_6	0.926	$P2_1/n$	5.42325(7)	5.54915(6)	7.7191(1)	89.918(1)
Sr_2CaMoO_6	0.919	$P2_1/n$	5.76151(5)	5.84449(5)	8.18437(8)	89.802(1)
Sr_2CaWO_6	0.917	$P2_1/n$	5.76861(6)	5.85008(6)	8.19467(9)	90.166(1)
Ca_2CaWO_6	0.867	$P2_1/n$	5.5518(3)	5.8100(3)	8.0066(4)	89.808(1)

Table 7
Selected bond distances, bond angles, bond valence sums, and octahedral distortion indices as determined from the crystallographic data reported in Tables 1–4.

	Ba_2MgWO_6	Ba_2CaMoO_6	Ba_2CaWO_6	Sr_2ZnMoO_6	Sr_2ZnWO_6	Ca_2CaWO_6
Bond distances (Å) and angles (deg.)						
A–O(1)	12 × 2.86820(7)	12 × 2.96847(3)	4 × 2.9752(4)	4 × 2.7949(1)	2.626(5)	2.765(2)
					2.737(6)	2.710(2)
					2.839(6)	2.351(1)
A–O(2)	–	–	4 × 2.923(2)	4 × 2.6281(4)	2.747(6)	2.960(2)
			4 × 3.027(2)	4 × 3.0042(5)	2.587(6)	2.368(1)
					2.841(6)	2.592(1)
A–O(3)	–	–	–	–	2.880(4)	2.389(1)
					2.757(4)	2.327(1)
					2.542(3)	3.382(1)
M^{2+}–O(1)	6 × 2.1245(4)	6 × 2.2782(4)	2 × 2.296(5)	2 × 2.087(1)	2 × 2.083(3)	2 × 2.2715(8)
M^{2+}–O(2)	–	–	4 × 2.273(3)	4 × 2.071(1)	2 × 2.088(3)	2 × 2.3317(8)
M^{2+}–O(3)	–	–	–	–	2 × 2.082(5)	2 × 2.3080(8)
M^{6+}–O(1)	6 × 1.9294(4)	6 × 1.9119(4)	2 × 1.904(5)	2 × 1.906(1)	2 × 1.915(3)	2 × 1.9155(8)
M^{6+}–O(2)	–	–	4 × 1.928(3)	4 × 1.915(1)	2 × 1.918(3)	2 × 1.9292(8)
M^{6+}–O(3)	–	–	–	–	2 × 1.920(5)	2 × 1.9316(9)
M^{2+}–O(1)–M^{6+}	180	180	176.0(1)	180	167.6(3)	147.22(4)
M^{2+}–O(2)–M^{6+}	–	–	–	164.5(4)	165.4(3)	140.94(4)
M^{2+}–O(3)–M^{6+}	–	–	–	–	164.1(1)	141.40(4)
Bond valence sums						
A	2.48	1.89	1.87	2.01	2.04	1.89
M^{2+}	1.87	2.59	2.57	2.19	2.15	2.42
M^{6+}	5.80	5.92	5.95	5.92	5.99	5.87
O(1)	2.10	2.05	2.10	2.00	2.03	2.05
O(2)	–	–	2.03	2.04	2.03	1.93
O(3)	–	–	–	–	2.05	2.06
Distortion indices (Δ_d; $\times 10^{-5}$)						
M^{2+}	–	–	2.26	1.31	0.16	11.6
M^{6+}	–	–	3.47	0.49	0.11	1.36

Table 8
Octahedral tilting at room temperature as a function of tolerance factor, *t*, and *A*-site cations for $A_2MM'O_6$ perovskites for M' = Nb, Ta, Mo, and W.

A	***M′***	$a^0a^0a^0$ (*Fm*$\bar{3}$*m*)	$a^0a^0c^-$ (*I*4/*m*)	$a^0b^-b^-$ (*I*2/*m*)	$a^-a^-c^+$ ($P2_1/n$)
Ba	Nb/Ta	$1.021 \geq t \geq 0.980$	$0.984 \geq t \geq 0.953$	$0.964 \geq t \geq 0.944$	–
Ba	Mo/W	$1.041 \geq t \geq 0.974$	$t = 0.972$	–	–
Sr	Nb/Ta	$1.020 \geq t \geq 1.018$	$0.992 \geq t \geq 0.974$	–	$0.963 \geq t \geq 0.949$
Sr	Mo/W	–	$0.982 \geq t \geq 0.979$	–	$0.976 \geq t \geq 0.917$
Ca	Nb/Ta	–	–	–	$0.963 \geq t \geq 0.878$
Ca	Mo/W	–	–	–	$0.926 \geq t \geq 0.867$

distortions seen for the CaO_6 octahedra are likely a reflection of two factors: the large octahedral tilting distortion, and the relatively ionic Ca–O bonds.

One of the interesting features of Table 7 is the consistency of the W–O and Mo–O bond lengths. Regardless of the identity of the other *M*-cation, the tungsten- and molybdenum-containing octahedra are consistently nearly ideal. This suggests that while the rest of the structure may distort, the $(Mo,W)O_6$ octahedra act as rigid units. This observation suggests that these compounds should be thought of as salts of the polyatomic MoO_6^{6-}/WO_6^{6-} ions.

Generalizations were previously made about octahedral tilting distortions in Nb^{5+}- and Ta^{5+}-containing double perovskites [9–13]. Combining that study with the results reported in this study allows for a thorough analysis of the tolerance factor boundaries that separate the cubic *Fm*$\bar{3}$*m* structure with no octahedral tilting, the tetragonal *I*4/*m* structure with $a^0a^0c^-$ tilting and the monoclinic $P2_1/n$ structure with $a^-a^-c^+$ tilting. The tolerance factor ranges over which each structure is observed at room temperature are tabulated in Table 8 and depicted graphically in Fig. 9. The cubic *Fm*$\bar{3}$*m* structure is found for tolerance factors ranging from 1.041 to 0.979, the tetragonal *I*4/*m* structure over the range 0.992–0.953, the monoclinic *I*2/*m* structure over the range 0.964–0.944, and the monoclinic $P2_1/n$ structure from 0.976 to 0.867. If we take $t = 0.97$ as the boundary between $a^0a^0c^-$ and $a^-a^-c^+$ tilting there is only one compound, Sr_2ZnMoO_6, that is not correctly sorted.

The boundary between $a^0a^0a^0$, $a^0a^0c^-$, and $a^0b^-b^-$ is more difficult to define. There are several examples of each tilt system for tolerance factors that fall in the range $1.00 < t < 0.96$. Three factors were considered as secondary factors in determining the most stable tilt system at room temperature: the identity of the *A* cation, the identity of the *M′* cation, and the difference in radii of the *M* and *M′* cations, ΔIR. Among these three, the data given in Table 8 and Fig. 9 clearly show that the identity of the *A* cation acts as the secondary structure directing factor. When *A* = Ba, the boundary between cubic and tetragonal symmetries falls near $t = 0.97$, whereas when *A* = Sr this boundary falls somewhere between $t = 1.018$ and $t = 0.992$. The previously noted flexibility in the Ba–O bond lengths likely plays a role in extending the stability of the cubic structure for Ba-containing double perovskites to lower values than might otherwise be expected.

Within the context of finding boundaries between different tilt systems those examples where otherwise identical Mo and W compounds have different symmetries, $Ba_2CaM'O_6$ and $Sr_2ZnM'O_6$, are quite interesting. Because heating is analogous to increasing the tolerance factor, these pairs of compounds must have

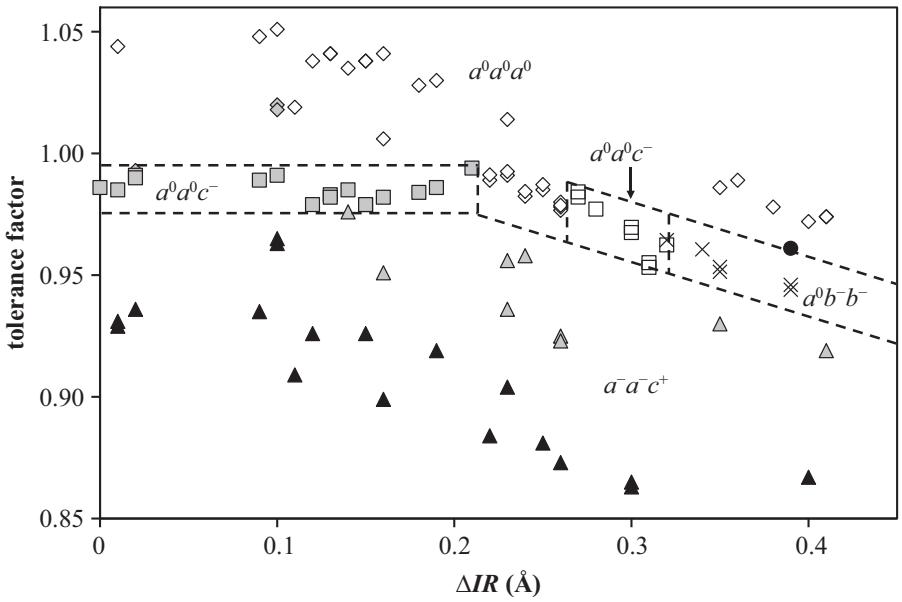

Fig. 9. A survey of the tolerance factor of 41 Mo/W- and 52 Nb/Ta-containing quaternary perovskites plotted as a function of the difference between the two six-coordinate *M*-cation ionic radii. Compounds with cubic symmetry are represented by diamonds, those with tetragonal symmetry are represented by squares, those with *I*2/*m* monoclinic symmetry are represented by ×, and those with $P2_1/n$ monoclinic symmetry are represented by triangles. White symbols represent compositions where $A=Ba^{2+}$, gray symbols represent compositions where $A=Sr^{2+}$, and black symbols represent where $A=Ca^{2+}$. The filled circle represents rhombohedral Ba_2BiTaO_6 ($t=0.961$; space group: $R\bar{3}$; tilt system: $a^-a^-a^-$). References for the compounds included in this figure are listed in the Supporting Information File.

transition temperatures near room temperature. In the first example, Ba_2CaMoO_6 has $Fm\bar{3}m$ space group symmetry whereas Ba_2CaWO_6 crystallizes with *I*4/*m* symmetry. The Ca^{2+}–O–W^{6+} bond angle in Ba_2CaWO_6 is nearly linear (176.0°), suggesting that the octahedral tilting along *c* is very subtle. This also suggests that with a small amount of heating, Ba_2CaWO_6 should undergo an *I*4/*m* to $Fm\bar{3}m$ phase transition. In the second example, Sr_2ZnMoO_6 has *I*4/*m* symmetry, yet Sr_2ZnWO_6 crystallizes with $P2_1/n$ symmetry. Here the presence of a phase transition close to room temperature is confirmed by the studies of Gateshki et al. who observed that Sr_2ZnWO_6 undergoes a phase transition from $P2_1/n$ to *I*4/*m* at 70 °C [35]. It is important to note that *I*2/*m* is regularly observed as an intermediate space group between *I*4/*m* and $P2_1/n$. However, it does not appear that any of the compositions examined in this work crystallize with *I*2/*m* symmetry. This observation cannot be explained.

5. Conclusions

Space group assignments and unit cell dimensions for seventeen A_2MMoO_6 and A_2MWO_6 ordered perovskites were determined from analysis of monochromatic laboratory X-ray and neutron diffraction data. These results, combined with earlier studies of A_2MNbO_6 and A_2MTaO_6 ordered perovskites, show that double perovskites containing Ba^{2+} with tolerance factors greater than 0.974 prefer cubic ($Fm\bar{3}m$) symmetry. In contrast, double perovskites containing Sr^{2+} with tolerance factors between 0.975 and 1 crystallize with tetragonal (*I*4/*m*) symmetry. Finally, compositions with tolerance factors below ~0.97 universally crystallize with monoclinic (*I*2/*m* or $P2_1/n$) symmetry.

Acknowledgments

We acknowledge the support of Argonne National Laboratory and the Intense Pulsed Neutron Source (IPNS) for providing the neutron research facilities used in this work. The authors acknowledge the National Science Foundation supported Center for Emergent Materials at The Ohio State University, an NSF MRSEC (Award # DMR-0820414), and Millikin University for financial support. We would also like to acknowledge Maxim Avdeev (Bragg Institute at the Australian Nuclear Science and Technology Organisation) for helpful discussions when analyzing the NPD data and Keenan Dungey (Department of Chemistry at the University of Springfield) for the use of their X-ray powder diffractometer.

Appendix A. Supporting materials

Supplementary data associated with this article can be found in the online version at doi:10.1016/j.jssc.2011.11.007.

References

[1] H.W. Eng, P.W. Barnes, B.M. Auer, P.M. Woodward, J. Solid State Chem. 175 (2003) 94.
[2] A. Hiskia, A. Troupis, S. Antonaraki, E. Gkika, P. Kormali, E. Papaconstantinou, Int. J. Environ. Anal. Chem. 86 (2006) 233.
[3] M.T. Anderson, K.B. Greenwood, G.A. Taylor, K.R. Poeppelmeier., Prog. Solid State Chem. 22 (1993) 197.
[4] P.K. Davies, Curr. Opin. Solid State Mater. Sci. 4 (1999) 467.
[5] R.H. Mitchell, Perovskites Modern and Ancient, Almaz Press, Thunder Bay, MI, 2002.
[6] M.W. Lufaso, P.W. Barnes, P.M. Woodward, Acta Crystallogr. B62 (2006) 387.
[7] C.J. Howard, B.J. Kennedy, P.M. Woodward, Acta Crystallogr. B59 (2003) 463.
[8] A.M. Glazer, Acta Crystallogr. B28 (1972) 3384.
[9] P.W. Barnes, M.W. Lufaso, P.M. Woodward, Acta Crystallogr. B62 (2006) 384.
[10] W.T. Fu, D.J.W. IJdo, J. Solid State Chem. 179 (2006) 1022.
[11] P.J. Saines, B.J. Kennedy, M.M. Elcombe, J. Solid State Chem. 180 (2007) 401.
[12] P.J. Saines, J.R. Spencer, B.J. Kennedy, M. Avdeev, J. Solid State Chem. 180 (2007) 2991.
[13] B.J. Kennedy, P.J. Saines, Y. Kubota, C. Minakata, H. Hano, K. Kato, M. Takata, Mater. Res. Bull. 42 (2007) 1875.
[14] R.W. Cheary, A. Coelho, J. Appl. Crystallogr. 25 (1992) 109.
[15] J.D. Jorgensen, J. Faber Jr., J.M. Carpenter, R.K. Crawford, J.R. Haumann, R.L. Hitterman, R. Kleb, G.E. Ostrowski, F.J. Rotella, T.G. Worlton, J. Appl. Crystallogr. 22 (1989) 321.
[16] A.C. Larson, R.B. Von Dreele, Los Alamos Natl. Lab., LAUR 86–748, (1994).

[17] B.H. Toby., J. Appl. Crystallogr. 34 (2001) 210.
[18] M.W. Lufaso, P.M. Woodward, Acta Crystallogr. B57 (2001) 725.
[19] E.G. Steward, H.P. Rooksby, Acta Crystallogr. 4 (1951) 503.
[20] I.N. Belyaev, V.S. Filip'ev, E.G. Fesenko, Zhurnal Strukturnoi Khimii 4 (1963) 719.
[21] E.G. Fesenko, V.S. Filip'ev, M.F. Kupriyanov, Izv. Akad. Nauk SSSR Fizi. 28 (1964) 669.
[22] K.S. Filip'ev, G.E. Shatalova, E.G. Fesenko, Kristallografiya 19 (1974) 386.
[23] D.D. Khalyavin, J.P. Han, A.M.R. Senos, P.Q. Mantas, J. Mater. Res. 18 (2003) 2600.
[24] S.J. Patwe, S.N. Achary, M.D. Mathews, A.K. Tyagi, J. Alloys Compd. 390 (2005) 100.
[25] N.-S. Chiu, S.H. Bauer, Acta Crystallogr. C40 (1984) 1646.
[26] D.E. Bugaris, J.P. Hodges, A. Huq, H.-C. zur Loye, J. Solid State Chem. 184 (2011) 2293.
[27] W.T. Fu, S. Akerboom, D.J.W. IJdo, J. Solid State Chem. 180 (2007) 1547.
[28] M.F. Kupriuanov, E.G. Fesenko, Kristallografiya 7 (1962) 451.
[29] R.H. Buttner, E.N. Maslen, Acta Crystallogr. B48 (1992) 764.
[30] A.M. Glazer, S.A. Mabud, Acta Crystallogr. B34 (1978) 1065.
[31] W.T. Fu, Y.S. Au, S. Akerboom, D.J.W. IJdo, J. Solid State Chem. 181 (2008) 2523.
[32] K. Yamamura, M. Wakeshima, Y. Hinatsu, J. Solid State Chem. 179 (2006) 605.
[33] E.J. Fresia, L. Katz, R. Ward, J. Am. Chem. Soc. 81 (1959) 4783.
[34] D. Reinen, H.O. Wellern, J. Wegwerth, Z. Phys. B104 (1997) 595.
[35] M. Gateshki, J.M. Igartua, E. Hernandez-Bocanegra, J. Phys.: Condens. Matter 15 (2003) 6199.
[36] E.G. Steward, W.A. Runciman, Nature (London) 172 (1953) 75.
[37] J.A. Baglio, S. Natansohn, J. Appl. Cryst. 2 (1969) 252.
[38] I.D. Brown, D. Altermatt, Acta Cryst. B41 (1985) 244.
[39] J.A. Alonso, M.J. Martinez-Lope, M.T. Casais, M.T. Fernandez-Diaz, Inorg. Chem. 39 (2000) 917.
[40] K. Momma, F. Izumi, J. Appl. Crystallogr. 41 (2008) 653.